Published in final edited form as:
Int J Radiat Biol. 2008 December ; 84(12): 976–983. doi:10.1080/09553000802512568.

DNA double-strand breaks induced by decay of ^{123}I-labeled Hoechst 33342: Role of DNA topology

PICHUMANI BALAGURUMOORTHY, **KETAI WANG**, **S. JAMES ADELSTEIN**, and **AMIN I. KASSIS**
Department of Radiology, Harvard Medical School, Boston, MA, USA

Abstract

Purpose—To determine double-strand-break (DSB) yields produced by decay of minor-groove-bound ^{123}I-labeled Hoechst 33342 (^{123}IEH) in supercoiled (SC) and linear (L) forms of pUC19 DNA, to compare strand-break efficiency of ^{123}IEH with that of ^{125}IEH, and to examine the role of DNA topology in DSB induction by these Auger electron emitters.

Materials and methods—Tritium-labeled SC and L pUC19 DNA were incubated with ^{123}IEH (0–10.9 MBq) at 4°C. After ^{123}I had completely decayed (10 days), samples were analyzed on agarose gel, and single-strand-break (SSB) and DSB yields were measured.

Results—Each ^{123}I decay in SC DNA produces a DSB yield of 0.18 ± 0.01. On the basis of DSB yields for ^{125}IEH (0.52 ± 0.02 for SC and 1.62 ± 0.07 for L, reported previously) and dosimetric expectations, a DSB yield of ~0.5 (3 × 0.18) per ^{123}I decay is expected for L DNA. However, no DSB are observed for the L form, even after ~2×10^{11} decays of ^{123}I per μg DNA, whereas a similar number of ^{125}I decays produces DSB in ~40% of L DNA.

Conclusion—^{123}IEH-induced DSB yield for SC but not L DNA is consistent with the dosimetric expectations for Auger electron emitters. These studies highlight the role of DNA topology in DSB production by Auger emitters and underscore the failure of current theoretical dosimetric methods *per se* to predict the magnitude of DSB.

Keywords

DNA strand break; DNA topology; Auger electron; ^{123}I; ^{125}I

Introduction

Many radionuclides exhibit the Auger effect, a phenomenon which is characterized by the emission of a cascade of low-energy electrons (Auger 1925). The decay of such radioactive atoms is accompanied by the creation of a primary vacancy in the inner shell consequent to

Correspondence: P. Balagurumoorthy, PhD, Department of Radiology, 200 Longwood Avenue, Armenise Building Room 137, Harvard Medical School, Boston, MA 02115, USA. Tel: +1 (617) 432 3887. Fax: 617 432 2419. pbalagurumoorthy@hms.harvard.edu.

Declaration of interest: The authors report no conflicts of interest. The authors alone are responsible for the content and writing of the paper.

electron capture and/or internal conversion and leads to the emission of X-ray photons and monoenergetic Auger or Coster-Kronig electrons with energies ranging from a few eV to ~1 keV (Cole 1969, Pomplun et al. 1987, Kassis 2004). Auger electrons travel a short distance of 2 to 500 nm; therefore, they behave like high linear energy transfer (LET) radiation (~2 to ~25 keV/μm) and must be in close proximity to DNA, to cause cytotoxicity (Sastry and Rao 1984, Charlton et al. 1987, Kassis 2004).

Among the Auger electron emitters, Iodine-125 and iodine-123 have attracted considerable attention in the development of cancer therapy (Bloomer and Adelstein 1977, Kassis et al. 1998, Kassis 2004, Kassis et al. 2004). The similar size of an iodine atom and a $–CH_3$ group has permitted the *in vivo* incorporation of radioiodine – as 5-[^{125}I/^{123}I]iodo-2′-deoxyuridine (^{125}IUdR, ^{123}IUdR) in the place of thymidine – into the nuclear DNA during cell division, thus facilitating the proximity of the decaying radioactive iodine atom to the DNA strand and inducing cell kill (Hofer and Hughes 1971, Feinendegen 1975, Chan et al. 1976, 1977, Makrigiorgos et al. 1989). Iodine-125-labeled DNA intercalators (Martin 1977, Kassis et al. 1989), ^{125}I-labeled benzimidazole minor-groove binders such Hoechst 33342 and 33258 (Martin and Holmes 1983, Kassis et al. 1999a, 1999b, 2000), ^{123}I-labeled steroid hormones (DeSombre et al. 1992, DeSombre et al. 2000), ^{125}I-internalizing antibodies and ^{125}I-deoxycytidine in homopyrimidine triplex-forming oligonucleotides (Panyutin et al. 2000, 2001) have also been used in positioning radioiodine decay proximal to the DNA in the nucleus.

Historically, radioiodine has been useful in the diagnosis and treatment of thyroid-related diseases (Rawson et al. 1951). Recently, ^{123}I, which emits a 159 keV γ-photon, has emerged as an alternative for thyroid imaging by single photon emission computed tomography (SPECT) (Reynolds and Robbins 1997, Yaakob et al. 1999). Unlike ^{131}I, the decay of ^{123}I does not emit β-particles and, therefore, delivers less radiation to the surrounding normal tissue. However, when ^{123}I is proximal to nuclear DNA, the cytotoxicity of Auger electron cascade could be a nuisance in ^{123}I imaging. Hence, a clear understanding of the mechanisms underlying ^{123}I induced DNA damage and cell death is necessary in developing reliable radiation safety tools to protect normal cells from radiation risk during these diagnostic procedures.

We have been interested in exploring the biophysical mechanisms underlying DNA damage induced by Auger emitters, particularly ^{125}I and ^{123}I. We had hypothesized that DNA compaction favors the formation of >1 DSB by $^{\bullet}$OH-mediated indirect mechanisms when DNA-incorporated ^{125}I decays (Walicka et al. 1998). Consequently, a higher DSB was expected for the supercoiled (SC) form of naked plasmid DNA due to its compacted state than for its torsionally relaxed, non-supercoiled counterpart, the linear (L) form. However, our recent study (Balagurumoorthy et al. 2008) using the minor-groove binder ^{125}I-labeled *m*-iodo-*p*-ethoxyHoechst 33342 (^{125}IEH) showed that supercoiling of naked plasmid DNA significantly reduces the magnitude of ^{125}I-induced DSB yield and affects the mechanism (direct versus indirect) of DSB production. A 3-fold higher DSB yield is observed for torisonally relaxed L DNA (~1.6 per decay of ^{125}I) than for SC DNA (~0.5 per ^{125}I decay), and both direct and indirect mechanisms produce DSB in the L form compared with only the direct mechanism in the SC form. In here, we compared ^{123}IEH-induced DSB yields for SC and L forms of pUC19 plasmid DNA and have analyzed the differences in the magnitude and mechanism of Auger-electron-induced DSB yield on DNA topology observed recently for ^{125}I.

Materials and methods

Synthesis of ^{123}I-/^{125}I-labeled m-iodo-p-ethoxyHoechst 33342 (^{123}IEH/^{125}IEH)

The radioiodinated (^{123}I/^{125}I) analogs of the DNA minor-groove-binding drug *m*-iodo-*p*-ethoxyHoechst 33342 (^{123}IEH/^{125}IEH) were synthesized from its trimethylstannyl derivative (Harapanhalli et al. 1996, Kassis et al. 1999a). In essence, carrier-free, dried Na^{123}I powder (370 MBq) in 0.1 M NaOH, purchased from MDS Nordion (Ottawa, Canada) was neutralized with 0.1 M HCl, and the pH of the solution was adjusted to ~7. To a vial coated with iodogen (5 μg), trimethylstannylHoechst 33342 (1 μl, 3μg/μl in dimethyl sulfoxide (DMSO), 0.1X phosphate buffered saline (PBS) (2 μl, pH 7.4), and Na^{123}I (11 μl, 185 MBq, ~8,800 TBq/mmole) were added, and the mixture was vortexed for 2 min at room temperature. The radioiodination was followed by analyzing 0.5-μl aliquots of reaction mixture on HPLC (Waters, Milford MA) with a reverse phase Zorbax SB C_{18} column (9.4 × 250 mm) (Harapanhalli et al. 1996, Kassis et al. 1999a). The radioiodinated product was identified using the retention time of nonradioactive (^{127}I) iodoHoechst 33342 run under identical conditions. Ultra-violet (UV) absorption (Waters 486 detector) and γ-ray emission (gamma-ram, IN/US Systems) were used to detect non-radioiodinated and radioiodinated products, respectively. Fractions containing ^{123}I-labeled Hoechst 33342 were collected, dried, and redissolved in water. The radiochemical yield was 85% and the radiochemical purity >98%. Since the retention times of Na^{123}I, ^{123}IEH, and Hoechst 33342, are distinct, the specific activity of the ^{123}I-labeled derivative is ~8,800 TBq/mmole. ^{125}IEH was synthesized in a similar fashion using Na^{125}I (Perkin Elmer Life and Analytical Sciences, Waltham MA, USA).

Preparation of ^{3}H-pUC19 plasmid DNA

pUC19 plasmid DNA (30 ng, New England Biolabs, Incorporated, Beverly MA, USA) was transformed into *Escherichia coli DH5α* competent cells (Invitrogen Incorporated, Gibco BRL, CA). Plasmid DNA was isolated from bacterial cultures grown for 16 h at 37°C in the presence of ^{3}H-thymidine (^{3}H-TdR, 370 KBq/ml) and ampicillin (50 μg/ml) (Balagurumoorthy et al. 2006). The medium was centrifuged at 6000 rpm in a GSA rotor, and the plasmid (^{3}H-pUC19) was isolated from the bacterial cell pellet using the Qiagen Plasmid Maxi kit. DNA was precipitated with ethanol and redissolved in PBS, (pH 7.4). DNA concentration was determined spectrophotometrically from absorbance at 260 nm. Agarose gel electrophoresis indicated that >99% of the DNA is in the SC state.

Linearization of ^{3}H-pUC19 plasmid DNA

Supercoiled ^{3}H-pUC19 plasmid DNA (100 μg in 134 μl 1X PBS, pH 7.4) was digested with EcoRI (1,000 units, 50 μl) in EcoRI buffer (1×, 500 μl, New England Biolabs Inc, Beverly MA, USA) for 16 h at 37°C. Linear (L) DNA formation in the reaction mixture was assessed on 1% agarose gel, another 100 units of EcoRI was added, and the incubation was continued for 12 h longer at 37°C. Subsequent agarose gel analysis indicated 100% linearization and no residual SC DNA left undigested. The reaction mixture was extracted twice with equal volumes of phenol equilibrated with Tris buffer (pH >7.5) and once with chloroform:isoamyl alcohol (24:1, v/v). Linear ^{3}H-pUC19 DNA was precipitated with ethanol, and the dried DNA pellet was redissolved in PBS (1 ×, 200 μl, pH 7.4). DNA concentration, measured spectrophotometrically from absorbance at 260 nm, was 0.375 μg/μl; the total yield was ~75 μg.

Incubation of supercoiled and linear forms of ^{3}H-pUC19 plasmid DNA with m-[^{123}I]iodo-p-ethoxyHoechst 33342 (^{123}IEH)

The pUC19 plasmid DNA concentration used in the ^{123}IEH–DNA (SC or L) incubations is 0.053 μM (1.8 μg, or 1.06 pmoles, in 20 μl), which is the same as that used in our previous studies with ^{125}IEH. The highest dose 10.9 MBq corresponds to 1.2 pmoles of ^{123}IEH.

Individual incubations of DNA with increasing amounts of ^{123}IEH (in the range of 0–10.9 MBq) in PBS at 4°C were continued for two weeks. Then aliquots (6 μl) were removed from the incubation mixtures, combined with 3 μl loading-dye-glycerol mixture and 3 μl PBS, and loaded onto 1% agarose gel in Tris-acetate-EDTA (TAE) buffer (0.5X) containing ethidium bromide (0.5 μg/ml). We estimate that the random pipetting error in loading the samples on the agarose gel is 3–7% of the total volume of the sample (12 μl). The gels were run at 200 volts (~7 volts/cm) and photographed on a transilluminator (long wave) attached to a charge coupled device (CCD) camera. For SC DNA–^{123}IEH incubations, DNA bands corresponding to SC, N (nicked-circular), and L forms were excised; for L DNA–^{123}IEH incubations, bands corresponding to intact L DNA were excised. The gel pieces were dissolved in scintillation cocktail (OPTI-FLOR) and ^{3}H content was determined by scintillation counting.

Calculation of ^{123}IEH-induced double-strand breaks in supercoiled and linear forms of ^{3}H-pUC19 plasmid DNA

The fraction of SC DNA remaining intact at each time point is plotted as a function of number of ^{123}IEH decays/ml. The number of ^{123}I disintegrations required to reduce the total number of DNA molecules initially present to 37% is defined by $D_0 = [(\log_{10} 37) - \log_{10} 100]/X$, where X is the slope obtained from the linear regression of the semilogarithmic plot. Since at zero decay, the fraction of intact DNA equals unity, the regression line is forced through 1. Statistically this is permissible because, in the absence of forcing through one, the *y* intercept is not significantly different. The strand-break calculations are based on the assumption that the binding of ^{123}IEH to DNA and, hence, the strand breaks, follow Poisson distribution.

The mean number of double (X_{DSB})-strand breaks per SC DNA molecule are calculated from the experimentally observed fractions of L DNA formed after exposure to a given number of ^{123}I disintegrations, using the following relationship (Cowan et al. 1987):

$$X_{DSB} = F_L/(1 - F_L),$$

where F_L is the fraction of L DNA formed as a result of exposure to accumulated ^{123}IEH decays (Kassis et al. 1999a, 1999b).

For the L form, the rate of formation of DSB must be equal to the rate of L DNA disappearance, as DSB are the only cause of reduction in intact L DNA band intensity. The mean number of DSB (X_{DSB}) per L DNA molecule are determined from the experimentally observed fractions of fragmented L DNA formed and intact L DNA remaining after exposure to a given number of disintegrations:

$$X_{DSB} = F_f/F_i,$$

where F_i is the fraction of intact L DNA remaining at any given time (ratio of ^{3}H dpm in intact L DNA remaining after ^{123}IEH-exposure to that in unirradiated control L DNA band), and F_f is the fraction of fragmented DNA occurring as a result of DSB due to ^{123}I decays ($1 - F_i$).

The rate of formation of DSB per DNA molecule per decay of ^{123}I is obtained by plotting X_{DSB} as a function of the number of accumulated ^{123}I decays per ml. We have carried out duplicate experiments and plotted them together in such a way as to nullify random errors associated with pipetting, loading, and recovery of samples. The standard errors obtained for the slopes of the linear regressions reflect such random pipetting, loading, and recovery errors. The straight lines are forced through zero, as at zero decay there would be neither single- nor double-strand breaks. The slopes of these linear regressions reflect DSB yield expressed as

number of DSB generated in one DNA molecule per decay of ^{123}I in one ml, and the reciprocal of the slopes represents D_0, the number of decays per ml required to form one DSB in one DNA molecule. The slope, when multiplied by the total number of plasmid DNA molecules per ml, gives the yield of DSB per decay of ^{123}I:

$$Y_{DSB}/^{123}\text{IEHdecay}=[\text{DNA}]/D_0,$$

where [DNA]=3.06 × 10^{13} molecules/ml.

Results and discussion

Detection of ^{123}IEH-induced double strand breaks in supercoiled ^{3}H-pUC19 plasmid DNA

Supercoiled ^{3}H-pUC19 DNA was incubated with ^{123}IEH for two weeks to allow complete decay of all the ^{123}I atoms present, and the DNA was analyzed on 1% agarose gels (Figure 1). Under the experimental conditions in these studies, the number of ^{123}I atoms per plasmid DNA molecule is 0.3 for the lowest added dose (2.8 MBq) and 1.2 for the highest dose (10.9 MBq) of ^{123}IEH. The gels show that SC DNA does not undergo strand breakage in the absence of ^{123}IEH during the course of incubation (Figure 1, Lane 1). However, there is a gradual decrease in fluorescence intensity of the SC DNA bands with increases in ^{123}IEH doses (Figure 1, lanes 2–6). The disappearance of SC DNA is accompanied by a concomitant appearance of N and L DNA indicating that the decay of ^{123}IEH causes both SSB and DSB in SC pUC19 plasmid DNA.

Quantitative analysis of DNA strand breaks in supercoiled ^{3}H-pUC19 DNA

The bands corresponding to SC, N and L forms of DNA in each lane in the agarose gel shown in Figure 1 were excised and the fraction of the DNA in each of these topological forms was determined by assaying the associated tritium content. Analysis of the fractions of SC, L and N present at various doses of ^{123}I reveals that: (i) At the lowest dose when the number of ^{123}I atoms decayed per plasmid molecule is 0.3, ~15% of the SC DNA disappear, producing ~6% L and ~9% N forms. A similar trend is observed even at the highest dose at which the number of ^{123}I atoms decayed per DNA molecule is ~1.2. At this ^{123}IEH:DNA ratio, ~50% of SC molecules disappear producing ~20% L and ~30% N forms through DSB and SSB, respectively.

Double-strand break yields are calculated using the method of Cowan et al. (1987). Figure 2A shows the disappearance of SC DNA as a function of ^{123}IEH decays. The D_0 for ^{123}IEH-decay-induced disappearance of SC DNA, calculated from the slope of the linear regression (Figure 2A) is (6.15 ± 0.19) × 10^{13} decays/ml, which is ~7 times higher than the D_0 for ^{125}IEH-induced disappearance of SC DNA (Balagurumoorthy et al. 2006).

The rate of formation of L DNA following DSB in SC DNA as a function of ^{123}IEH decays is shown in Figure 2B. The D_0 of (16.64 ± 0.67) × 10^{13} decays/ml for the formation of the L form is ~3-fold higher than that induced by ^{125}IEH decays (Balagurumoorthy et al. 2006). Accordingly, the DSB yield for ^{123}IEH (0.18 ± 0.01) is 3-fold lower than that generated by ^{125}IEH decays (Table I). This 0.18 DSB/^{123}I decay yield is ~3 times lower than that reported by Lobachevsky and Martin (2005) when SC DNA from a different plasmid (pBR322) was incubated with another Hoechst analog, ^{123}I-iodoHoechst 33258 (^{123}IMH). These authors also reported the ratio of DSB yields induced by the two Auger electron emitters ^{123}I and ^{125}I as 0.77 (^{123}IMH: 0.62 DSB/decay; ^{125}IMH: 0.82 DSB/decay), a value that differs from the ratio of 0.33 obtained when the DSB yields after ^{123}IEH (current studies) and ^{125}IEH (Balagurumoorthy et al. 2006) are compared. These differences may be attributed to the subtle

dissimilarities in the plasmid DNA model (pUC19 vs. pBR322), the two carrier Hoechst ligands used (IEH vs. IMH), each with its binding specificity and affinity, and/or variation in experimental conditions. However, our finding that ^{125}IEH is ~3 times more efficient than ^{123}IEH in inducing DNA DSB in naked SC plasmid DNA (in comparison to the 1.3 value reported for IMH) is in line with our previous experimental studies in which ^{125}I was ~ 2.2 times more efficient than ^{123}I in causing DNA DSB in mammalian DNA (Makrigiorgos et al. 1992), a value that is also similar to the ratios obtained when the energy deposited in small spheres (2–50 nm radius) around decaying ^{125}I and ^{123}I atoms is estimated using semiempirical Monte Carlo calculations (Makrigiorgos et al. 1989).

^{123}IEH-induced double-strand-breaks in linear DNA

We have recently examined the effect of DNA topology on the mechanism and magnitude of DSB produced in plasmid pUC19 DNA by ^{125}IEH (Balagurumoorthy et al. 2008) and γ rays (unpublished results). The data indicate that DSB yield is influenced by DNA topology for both types of radiation. For example, the DSB yield per DNA molecule following γ-ray irradiation of L DNA ($[30.9 \pm 2.17] \times 10^{-4}$/Gy) is ~2.4-fold higher that obtained with SC DNA ($[13.0 \pm 0.51] \times 10^{-4}$/Gy). Similarly, ^{125}IEH-induced DSB yield in the L form (1.62 ± 0.07) is 3-fold higher than that in the SC form (0.52 ± 0.02). These results lead us to conclude that DNA topology affects the DSB yield following γ-irradiation or ^{125}I decay in close proximity to DNA.

In analogy with these latter findings, we expected each decay of ^{123}IEH in L DNA to generate a 2- to 3-fold higher DSB yield (0.4–0.6 DSB/decay) than that obtained for SC DNA (0.18 ± 0.01). However, when L DNA samples were incubated with the same ^{123}IEH concentration and run on 1% agarose gel, we could not detect any reduction in the fluorescence intensity of the intact L DNA band due to DSB (Figure 3, lanes 1–5), except for the faint smear seen in the lanes (insignificant compared to the total amount of DNA present in the lanes). These observations indicate that, within the radioactive concentrations used, the decay of ^{123}IEH is either unable to or minimally able to induce DSB. This conclusion is supported by our data (^{3}H-TdR counts in excised fluorescent L DNA band) showing that the amount of intact L DNA present in the gels is not reduced following exposure to ^{123}IEH. Consequently, when the fractions of L DNA remaining post irradiation are plotted as a function of ^{123}IEH decays/ml (Figure 4), a very shallow slope (6.2×10^{-5}) is obtained (essentially, there is no quantifiable decrease in the amount of L DNA). For comparison, the rapid rate at which DNA disappears following exposure of L DNA to ^{125}IEH decays (under similar experimental conditions) is shown as a dotted line (Balagurumoorthy et al. 2008). Note that ~50% of the L DNA molecules exposed to $\sim 25 \times 10^{12}$ decays per ml ^{125}IEH have disappeared but that for a similar number of ^{123}IEH decays, ~100% of the L DNA is intact. Thus, unlike ^{125}IEH which induces DSB in both SC and L DNA, ^{123}IEH induces DSB only in the SC form.

To confirm these observations, the disappearance of L DNA following exposure to the same number of ^{123}IEH and ^{125}IEH decays ($\sim 2 \times 10^{11}$) was compared. The results (Figure 5) show that the fluorescence intensity of intact L DNA band after ^{125}I decays is clearly diminished when compared with the DNA control band whereas nearly 100% of L DNA remains intact after being irradiated with the same number of ^{123}IEH decays (very similar to the unirradiated pUC19 L DNA controls). When the amount of L DNA in each band was quantified, the data demonstrate that exposure to 2×10^{11} ^{125}IEH decays leads to the disappearance of ~50% of L DNA (due to DSB) whereas > 95% of ^{123}I-exposed DNA is still present as L DNA.

We have no ready explanation for the failure of ^{123}I decay to produce DSB in L DNA. ^{123}I differs from ^{125}I in several ways: The latter decays in two steps –electron capture (EC) and internal conversion (IC); each step produces an average of ~10 low-energy electrons. Iodine-123 decays by EC alone, producing ~10 electrons only. Consequently, ^{125}I builds up

twice the positive charge as that of ^{123}I and the dissipation of the potential energy associated with the higher positive charge of the residual ^{125}I atom and its neutralization may, in principle, also act concomitantly and be responsible for the differences in the observed effects. In addition the decay constant for ^{123I}I is considerably greater than that for ^{125}I, i.e., ^{123}I has a much shorter half-life.

We can only speculate on some of the possible reasons underlying this unexpected finding (Table II): (1) The DSB yield following the decay of the two iodine isotopes is the same for the common EC step – 0.2 in SC DNA and 0.0 in L DNA; (2) the differences in total DSB yield are mainly due to the IC step (^{125}I decay) − 0.3 and 1.6 DSB respectively for SC and L. Without IC decay, there are no subsequent DSB produced by ^{123}I.

What mechanisms might prevent the EC step from producing DSB in L DNA? Obviously, the topology of the L DNA molecules, which differs from that of SC DNA, may play an important role, e.g., the greater stokes radius of the L form, the prominent curvatures within the compacted SC DNA molecules vs. the relaxed elongated linear structure of L DNA molecules. For example, the curvature could increase the DSB yield in SC DNA consequent to the positioning of some bases that are hundreds/thousands of angstroms away from the minor groove-bound decaying ^{123}IEH but within the range of emitted electrons and/or radicals formed along their tracks. Another possibility is electron tunneling/migration within double stranded DNA molecules, a phenomenon that leads to the induction of DNA lesions over long distances (Bixon et al. 1999, Nunez et al. 1999, Giese 2002, 2006). One can imagine that migration of emitted low energy Auger electrons within the plasmid DNA is more likely to damage SC DNA (with electrons being trapped within the circular structure and a higher probability of interacting with an atom within the DNA molecule and forming a break) than L DNA (with particles escaping from the termini of L DNA and thereby reducing the opportunity to interact with atoms within the DNA molecule and rupture it). Alternatively, to the extent that charge neutralization may also contribute to DSB production (Charlton et al. 1987, Kassis et al. 1987, Lobachevsky and Martin 2000), a greater charge may be necessary to fracture linear DNA than the supercoiled form. Clearly, further experimentation will be necessary to gain insights into the rationale behind this surprising phenomenon.

Conclusions

Comparison of DSB produced by ^{123}IEH and ^{125}IEH following their decay within the minor groove of plasmid SC DNA indicates that the DSB yield for these two Auger emitters is consistent with dosimetric expectations: ^{123}IEH is ~3 times less efficient than ^{125}IEH in inducing DSB, and this relative efficacy is in reasonable agreement with studies in mammalian cells using ^{123}IUdR and ^{125}IUdR. That ^{123}IEH decay does not induce DSB in the relaxed L form whereas ^{125}IEH decay leads to a 3-fold increase in DSB yield (compared with the yield in SC DNA) highlights the important and unpredictable role of DNA topology (and other factors) in DSB production by Auger emitters. This observation underscores the failure of current dosimetric methods to predict the magnitude of DSB. The current work suggests the need for developing more comprehensive models that include DNA structure and topology for examining the biophysical mechanisms underlying DSB produced by Auger emitters.

Acknowledgments

This work was supported in part by NIH 5 R01 CA15523 (Amin I. Kassis) and NIH 5 T32 CA009078 (Pichumani Balagurumoorthy).

References

Auger P. Sur les rayons b secondaires produits dans un gaz par des rayons X. Comptes Rendues Hebdomadaires des Seances de l'Academie des Sciences 1925;180:65–68.

Balagurumoorthy P, Chen K, Adelstein SJ, Kassis AI. Auger electron-induced double-strand breaks depend on DNA topology. Radiation Research 2008;170:70–82. [PubMed: 18582152]

Balagurumoorthy P, Chen K, Bash RC, Adelstein SJ, Kassis AI. Mechanisms underlying production of double-strand breaks in plasmid DNA after decay of ^{125}I-Hoechst. Radiation Research 2006;166:333–344. [PubMed: 16881734]

Bixon M, Giese B, Wessely S, Langenbacher T, Michel-Beyerle ME, Jortner J. Long-range charge hopping in DNA. Proceedings of the National Academy of Sciences of the USA 1999;96:11713–11716. [PubMed: 10518515]

Bloomer WD, Adelstein SJ. 5-^{125}I-iododeoxyuridine as prototype for radionuclide therapy with Auger emitters. Nature 1977;265:620–621. [PubMed: 859560]

Chan PC, Lisco E, Lisco H, Adelstein SJ. The radiotoxicity of iodine-125 in mammalian cells. II. A comparative study on cell survival and cytogenetic responses to ^{125}IUdR, ^{131}IUdR, and ^{3}HTdR. Radiation Research 1976;67:332–343. [PubMed: 948559]

Chan PC, Lisco E, Lisco H, Adelstein SJ. Cell survival and cytogenetic responses to ^{125}I-UdR in cultured mammalian cells. Current Topics in Radiation Research Quarterly 1977;12:426–435. [PubMed: 565273]

Charlton DE, Pomplun E, Booz J. Some consequences of the Auger effect: Fluorescence yield, charge potential, and energy imparted. Radiation Research 1987;111:553–564. [PubMed: 3659287]

Cole A. Absorption of 20-eV to 50,000-eV electron beams in air and plastic. Radiation Research 1969;38:7–33. [PubMed: 5777999]

Cowan R, Collis CM, Grigg GW. Breakage of double-stranded DNA due to single-stranded nicking. Journal of Theoretical Biology 1987;127:229–245. [PubMed: 2826926]

DeSombre ER, Hughes A, Hanson RN, Kearney T. Therapy of estrogen receptor-positive micrometastases in the peritoneal cavity with Auger electron-emitting estrogens: theoretical and practical considerations. Acta Oncologica 2000;39:659–666. [PubMed: 11130001]

DeSombre, ER.; Hughes, A.; Shafii, B.; Púy, L.; Kuivanen, PC.; Hanson, RN.; Harper, PV. Estrogen receptor-directed radiotoxicity with Auger electron-emitting nuclides: E-17a-[^{123}I] iodovinyl-11b-methoxyestradiol and CHO-ER cells. In: Howell, RW.; Narra, VR.; Sastry, KSR.; Rao, DV., editors. Biophysical aspects of Auger processes; American Association of Physicists in Medicine Symposium Series No. 8; Woodbury, NY: American Institute of Physics; 1992. p. 352-371.

Feinendegen LE. Biological damage from the Auger effect, possible benefits. Radiation and Environmental Biophysics 1975;12:85–99. [PubMed: 1101289]

Giese B. Long-distance electron transfer through DNA. Annual Review of Biochemistry 2002;71:51–70.

Giese B. Electron transfer through DNA and peptides. Bioorganic and Medicinal Chemistry 2006;14:6139–6143. [PubMed: 16784861]

Harapanhalli RS, McLaughlin LW, Howell RW, Rao DV, Adelstein SJ, Kassis AI. [^{125}I/^{127}I] iodoHoechst 33342: synthesis, DNA binding, and biodistribution. Journal of Medicinal Chemistry 1996;39:4804–4809. [PubMed: 8941394]

Hofer KG, Hughes WL. Radiotoxicity of intranuclear tritium, ^{125}iodine and ^{131}iodine. Radiation Research 1971;47:94–109. [PubMed: 5559387]

Kassis AI. The amazing world of Auger electrons. International Journal of Radiation Biology 2004;80:789–803. [PubMed: 15764386]

Kassis AI, Fayad F, Kinsey BM, Sastry KSR, Adelstein SJ. Radiotoxicity of a ^{125}I-labeled DNA intercalator in mammalian cells. Radiation Research 1989;118:283–294. [PubMed: 2727257]

Kassis AI, Harapanhalli RS, Adelstein SJ. Comparison of strand breaks in plasmid DNA after positional changes of Auger electron-emitting iodine-125. Radiation Research 1999a;151:167–176. [PubMed: 9952301]

Kassis AI, Harapanhalli RS, Adelstein SJ. Strand breaks in plasmid DNA after positional changes of Auger electron-emitting iodine-125: Direct compared to indirect effects. Radiation Research 1999b; 152:530–538. [PubMed: 10521930]

Kassis AI, Kirichian AM, Wang K, Safaie Semnani E, Adelstein SJ. Therapeutic potential of 5-[^{125}I] iodo-2′-deoxyuridine and methotrexate in the treatment of advanced neoplastic meningitis. International Journal of Radiation Biology 2004;80:941–946. [PubMed: 15764406]

Kassis AI, Sastry KSR, Adelstein SJ. Kinetics of uptake, retention, and radiotoxicity of ^{125}IUdR in mammalian cells: Implications of localized energy deposition by Auger processes. Radiation Research 1987;109:78–89. [PubMed: 3809393]

Kassis AI, Walicka MA, Adelstein SJ. Double-strand break yield following ^{125}I decay: Effects of DNA conformation. Acta Oncologica 2000;39:721–726. [PubMed: 11130010]

Kassis AI, Wen PY, Van den Abbeele AD, Baranowska-Kortylewicz J, Makrigiorgos GM, Metz KR, Matalka KZ, Cook CU, Sahu SK, Black PM, Adelstein SJ. 5-[^{125}I]iodo-2′-deoxyuridine in the radiotherapy of brain tumors in rats. Journal of Nuclear Medicine 1998;39:1148–1154. [PubMed: 9669385]

Lobachevsky PN, Martin RF. Iodine-125 decay in a synthetic oligodeoxynucleotide. II. The role of Auger electron irradiation compared to charge neutralization in DNA breakage. Radiation Research 2000;153:271–278. [PubMed: 10669548]

Lobachevsky PN, Martin RF. DNA breakage by decay of Auger electron emitters: experiments with ^{123}I-iodo-Hoechst 33258 and plasmid DNA. Radiation Research 2005;164:766–773. [PubMed: 16296882]

Makrigiorgos GM, Berman RM, Baranowska-Kortylewicz J, Bump E, Humm JL, Adelstein SJ, Kassis AI. DNA damage produced in V79 cells by DNA-incorporated iodine-123: A comparison with iodine-125. Radiation Research 1992;129:309–314. [PubMed: 1542718]

Makrigiorgos GM, Kassis AI, Baranowska-Kortylewicz J, McElvany KD, Welch MJ, Sastry KSR, Adelstein SJ. Radiotoxicity of 5-[^{123}I]iodo-2′-deoxyuridine in V79 cells: a comparison with 5-[^{125}I]iodo-2′-deoxyuridine. Radiation Research 1989;118:532–544. [PubMed: 2727274]

Martin RF. Induction of double-stranded breaks in DNA by binding with a ^{125}I-labelled acridine. International Journal of Radiation Biology 1977;32:491–497.

Martin RF, Holmes N. Use of a ^{125}I-labelled DNA ligand to probe DNA structure. Nature 1983;302:452–454. [PubMed: 6188059]

Nunez ME, Hall DB, Barton JK. Long-range oxidative damage to DNA: Effects of distance and sequence. Chemistry and Biology 1999;6:85–97. [PubMed: 10021416]

Panyutin IG, Winters TA, Feinendegen LE, Neumann RD. Development of DNA-based radiopharmaceuticals carrying Auger-electron emitters for anti-gene radiotherapy. Quarterly Journal of Nuclear Medicine 2000;44:256–267. [PubMed: 11105589]

Panyutin IV, Luu AN, Panyutin IG, Neumann RD. Strand breaks in whole plasmid DNA produced by the decay of ^{125}I in a triplex-forming oligonucleotide. Radiation Research 2001;156:158–166. [PubMed: 11448236]

Pomplun E, Booz J, Charlton DE. A Monte Carlo simulation of Auger cascades. Radiation Research 1987;111:533–552. [PubMed: 3659286]

Rawson RW, Rall JE, Peacock W. Limitations and indications in the treatment of cancer of the thyroid with radioactive iodine. Journal of Clinical Endocrinology and Metabolism 1951;11:1128–1142. [PubMed: 14873783]

Reynolds JC, Robbins J. The changing role of radioiodine in the management of differentiated thyroid cancer. Seminars in Nuclear Medicine 1997;27:152–164. [PubMed: 9144857]

Sastry, KSR.; Rao, DV. Dosimetry of low energy electrons. In: Rao, DV.; Chandra, R.; Graham, MC., editors. Physics of nuclear medicine: Recent advances. Woodbury, NY: American Institute of Physics; 1984. p. 169-208.

Walicka MA, Adelstein SJ, Kassis AI. Indirect mechanisms contribute to biological effects produced by decay of DNA-incorporated iodine-125 in mammalian cells *in vitro*: Clonogenic survival. Radiation Research 1998;149:142–146. [PubMed: 9457893]

Yaakob W, Gordon L, Spicer KM, Nitke SJ. The usefulness of iodine-123 whole-body scans in evaluating thyroid carcinoma and metastases. Journal of Nuclear Medicine Technology 1999;27:279–281. [PubMed: 10646545]

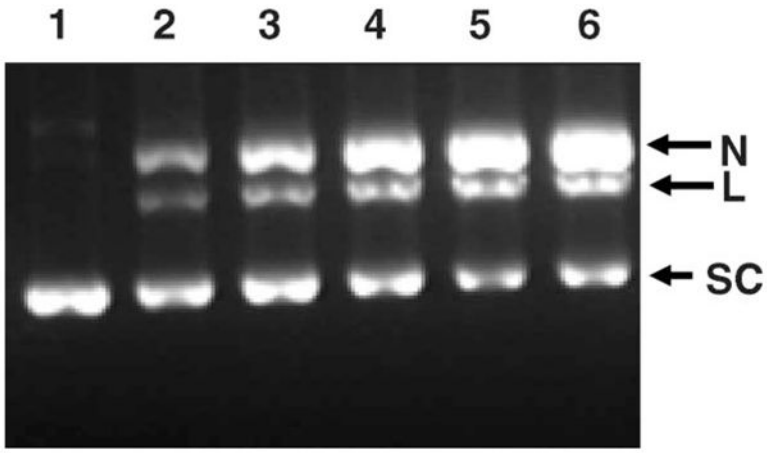

Figure 1.

Agarose gel analysis of SC ^{3}H-pUC19 plasmid DNA incubated with ^{123}IEH at 4°C in PBS (pH 7.4): lane 1, control (no ^{123}IEH); lane 2 9.7×10^{12} decays/ml; lane 3, 13.7×10^{12} decays/ml; lane 4, 23.5×10^{12} decays/ml; lane 5, 34.9×10^{12} decays/ml; and lane 6, 37.6×10^{12} decays/ml. Gels (containing ethidium bromide) were visualized using ultraviolet (320 nm) transillumination.

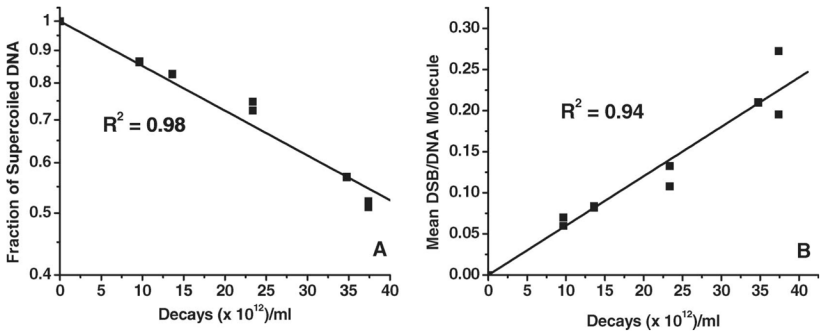

Figure 2.

Quantitative analysis of data from agarose gel electrophoresis assessing disappearance of SC ^{3}H-pUC19 plasmid DNA (A) and appearance of L DNA (B), indicator of DSB formation, as function of accumulated ^{123}I decays.

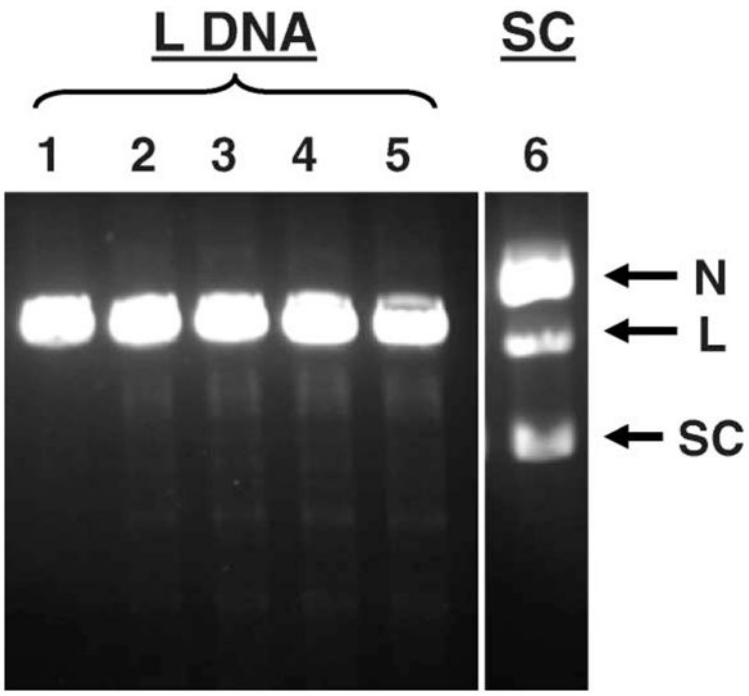

Figure 3.

Agarose gel analysis of L form of ^{3}H-pUC19 plasmid DNA incubated with ^{123}IEH at 4°C in PBS (pH 7.4): lane 1, control (no ^{123}IEH); lane 2, 4.6×10^{12} decays/ml; lane 3, 8.1×10^{12} decays/ml; lane 4, 11.5×10^{12} decays/ml; and lane 5, 21.9×10^{12} decays/ml, lane 6, SC DNA exposed at the highest dose (21.9×10^{12} decays/ml) showing DSB formation for comparison.

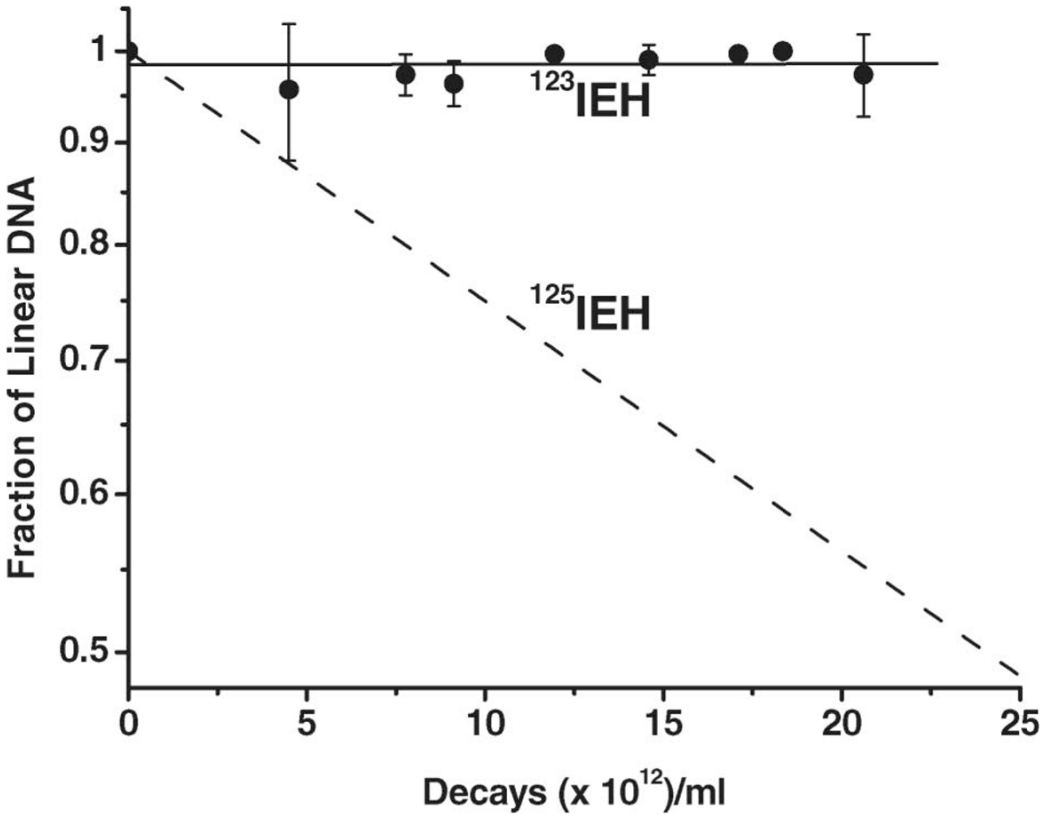

Figure 4.
Quantitative analysis of data obtained from agarose gel electrophoresis indicating disappearance of L ^{3}H-pUC19 plasmid DNA after exposure to ^{123}IEH (●). Error bars are the standard deviation of the mean for three independent experiments. Dotted line shows rate of disappearance of L DNA exposed to ^{125}IEH decays (Balagurumoorthy et al. 2008).

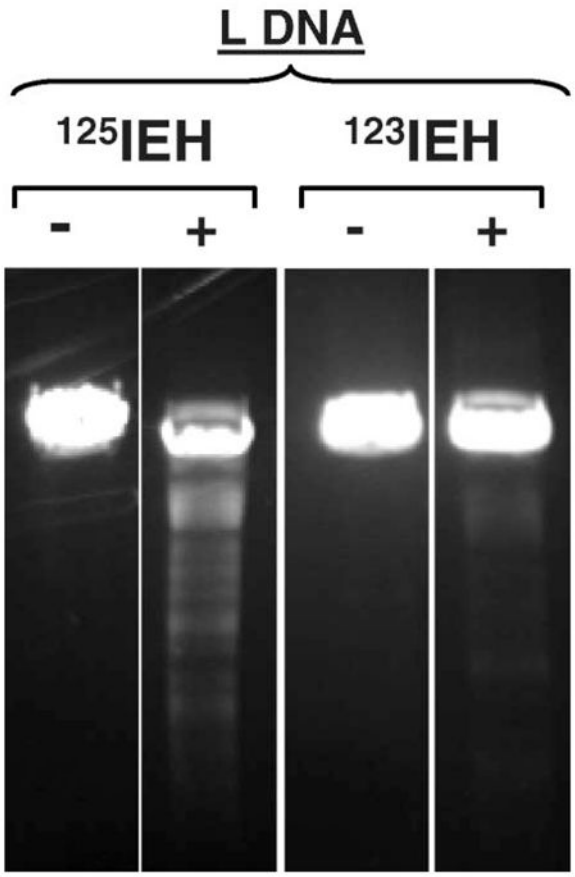

Figure 5.
Comparison of pUC19 L DNA exposed to the same number (~2×10^{11}) of ^{125}IEH and ^{123}IEH decays per μg DNA: (−) and (+) indicate absence and presence of radioiodinated ligand, respectively.

Table I

DSB yields in pUC19 SC and L plasmid DNA after decay of ^{123}I bound to minor groove (^{123}IEH): Comparison with ^{125}IEH.

	DSB/decay	
	SC	**L**
^{123}IEH	0.18 ± 0.01	0.00
^{125}IEH	0.55 ± 0.01*	1.620 ± 0.07*

*Data previously published (Balagurumoorthy *et al.* 2008). Standard errors are obtained from the slope of the linear regressions used to calculate the DSB yields.

Table II

Comparison of DSB yields among different plasmid DNA forms: Dependence of DNA topology.

						DSB per decay	
		1st step: EC	**2nd step: IC**	**Highly compacted Highly curved**	**Terminal nucleotide(s)**	**Experimental**	**Assigned***
SC	^{125}I	Yes	–	Yes	No	0.5	0.2
		–	Yes	Yes	Yes		0.3
	^{123}I	Yes	–	Yes	No	0.2	0.2
		–	No	NA	NA		NA
L	^{125}I	Yes	–	No	Yes	1.6	0.0
		–	Yes	No	Yes		1.6
	^{123}I	Yes	–	No	Yes	0.0	0.0
			No	NA	NA		NA

*Segregation calculated assuming the same DSB yields for both radionuclides following EC.